International Journal of Thermophysics (2023) 44:24
https://doi.org/10.1007/s10765-022-03132-8

Numerical Simulation of Internal Factors that Influence the Thermal Conductivity of Rock

Chuanqing Zhu[1,2] · **Chi Chen**[1,2,3] · **Xiaoxue Jiang**[1,2]

Received: 10 August 2022 / Accepted: 14 November 2022

Abstract

Rock thermophysical properties are the basic parameters that constrain the temperature field, thermal evolution, and thermal regime of the lithosphere. The petrofabric is the internal factor that most directly affects the thermal conductivities of rocks. In this study, we used the finite-element method to simulate the influence of major petrofabric characteristics such as pore size, fracture angle, and composition arrangement on the thermal conductivity. The results show that at the 1 % porosity there is no obvious relationship between pore size and thermal conductivity. However, the contact thermal resistance between grains is different in rocks with different pore sizes or grain sizes. Further, the angle between a fracture and the direction of heat flow has an obvious effect on the thermal conductivity of a rock, and the thermal conductivity decreases as this angle increases. It is thus necessary to pay attention to this angular relationship when modelling the effective thermal conductivity of rock with cracks developed. In addition, the arrangement of components in rocks affects both the thermal conductivity and the response of the thermal conductivity to temperature. We expect the present results to be helpful in understanding quantitatively the influence of these factors on the thermal conductivity of rock and to provide a valuable reference for experimental studies of rock thermal conductivity and strata thermal conductivity modelling.

Keywords Components arrangement · Fracture · Numerical simulation · Petrofabric · Porosity · Thermal conductivity

Abbreviations

T Temperature
k Thermal conductivity
q Heat flow

✉ Chuanqing Zhu
zhucq@cup.edu.cn

Extended author information available on the last page of the article

Published online: 03 December 2022

1 Introduction

The thermophysical properties of rocks are the fundamental parameters that constrain the Earth's temperature field and the thermal evolution and thermal state of the lithosphere. As one of the vital thermophysical properties, the thermal conductivity has an essential influence on heat transfer processes within the lithosphere. Accurate data for the rock thermal conductivity are thus important for understanding the thermal structure of the lithosphere and geodynamics. Besides, the distribution of the temperature field in the shallow crust is closely related to its thermal conductivity. Thermal conductivity studies also have crucial practical significance in the prevention and control of thermal damage in mines [1, 2], road-tunnel construction [3], geothermal-resource exploration [4, 5], and nuclear-waste protection [6].

In addition to external factors such as temperature and pressure, the composition of a rock is the internal factor that most directly affects its thermal conductivity. The rock fabric—including its mineral composition, porosity, degree of water saturation, particle size, particle shape, particle arrangement, particle distribution, particle orientation, pore structure, and specific surface area [7–9]—affects its thermal conductivity to different degrees. These factors are not easily characterized, and they interact, which complicates the relationship between the composition of a rock and its thermal conductivity [10]. It is therefore crucial to perform experimental studies and numerical simulations to study the factors that influence the thermal conductivities of rocks.

Pores and fractures are commonly found in rocks, and they are often filled with gases and/or liquids for which the thermal conductivity is much lower than that of the mineral particles in rocks. Thus, pores and fractures can significantly reduce the thermal conductivities of rocks. It is difficult to find an ideal series of samples for variable-parameter experiments to investigate the effects of pores and fractures on the thermal conductivities of rocks. This makes experimental research more complex, and it is therefore necessary to rely on numerical simulations to solve this problem. Nowadays, COMSOL, Analyzer, and other types of 3D simulation software can simulate rock structures, which significantly improves the convenience of simulations. In this work, we use COMSOL Multiphysics software to simulate the effects of major constitutive features such as pore size, fracture angle, and component arrangement on the thermal conductivities of rocks. Our study results can thus help to quantify the influence of these factors on the thermal conductivity of rock and can provide valuable references for experimental studies of the rock thermal conductivity and the modeling of strata thermal conductivity.

2 Modeling Methods and Simulation Results

We calculated the effective thermal conductivity by modeling the rock configuration in three dimensions through the finite-element method using COMSOL Multiphysics. We defined the mesh, set the thermal properties of the material

skeleton, and simulated the three-dimensional distribution of temperature within a rock model using the temperatures at the heat flow inlet and outlet interfaces as boundary conditions.

The finite-element method uses a finite number of independent cells to represent the overall heat-conduction domain, treats the appropriate nodes in each cell as interpolation points for solving the equations, defines the differential-equation variables through linear equations composed of node values and interpolation functions, and finally solves the differential equations using a weighted-residual method or a variational principle [11]. The finite-element method for heat transfer simulations has the following advantages [12–14]:

a. The program provides uniformity and flexibility: the computational steps are similar in simulations of various models, and the procedure can be quickly converted from solving one type of problem to another with simple and convenient programming and computational processes.
b. Grid dissection and solution are more suitable for complex boundary conditions, such as irregularly shaped boundaries, and for inhomogeneous or anisotropic objects.
c. Cells have diversity and flexibility. There is no particular restriction on cell dissection, and the size and shape of a cell can be determined according to the actual research situation and the scale and accuracy of the physical model.
d. The computational accuracy for heat-conduction events is higher than that obtainable with a finite-difference method.

2.1 Effect of Pore Size on Thermal Conductivity

2.1.1 Modeling

The negative correlation between the thermal conductivity and porosity of rock has been demonstrated in numerous experimental and theoretical studies; it occurs because rock pores are filled with low-thermal conductivity gas or liquid. In the present study, we have focused on simulating the effect of porosity size on thermal conductivity. We first established a 1 cm × 1 cm × 1 cm cube as the basic rock material, and we used the COMSOL Multiphysics App-developer language to create numerous non-overlapping ellipsoidal voids in it at random positions and oriented at random angles to simulate the pores in the rock. We fixed the ratio of the long axis/short axis of these ellipsoids to be 5, and we set the lengths of the semi-major axes to be 0.06 cm, 0.07 cm, 0.08 cm … 0.19 cm, and 0.20 cm, using a total of 15 different lengths to characterize different pore sizes. To keep the porosity constant for various lengths of the semi-major axis, we require that the total combined volume of these ellipsoidal volumes remains constant (see Fig. 1).

After each ellipsoid is randomly generated, if it overlaps with a previously created ellipsoid, it is recreated until there is no overlap among any of the ellipsoids. Setting the porosity constant at 1 %, we add up the volumes of the generated ellipsoids until the total volume of ellipsoids reaches 0.01 cm^3. We assumed

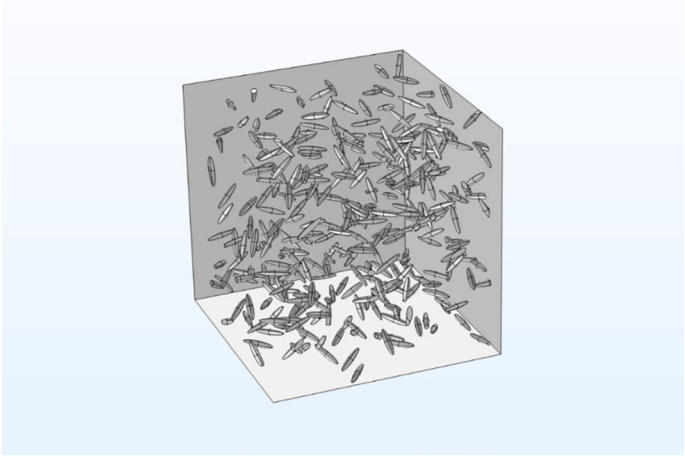

Fig. 1 Stochastic geometric modeling of pores

the thermal conductivity of the rock material to be 2.80 $W \cdot m^{-1} \cdot K^{-1}$, its density to be 2800 $kg \cdot m^{-3}$, and its mass-specific heat capacity to be 850 $J \cdot kg^{-1} \cdot K^{-1}$. We chose the material within each ellipsoid to be air (its heat capacity was assumed to be 1009 $J \cdot kg^{-1} \cdot K^{-1}$, and its thermal conductivity was assumed to be 2.373×10^{-2} $W \cdot m^{-1} \cdot K^{-1}$), and we set the temperature of the upper surface of the model to 273.15 K. The temperature of its lower surface was set as adiabatic surfaces to achieve one-way steady-state heat transfer. The physical-field control mesh is generated automatically by the software's scribing mesh function, and the program simulates the three-dimensional temperature distribution of the model (see Fig. 2). The model meshes have an average element quality of approximately 0.92 (maximum 1). In addition, each model was simulated three times under three different precisions of mesh, while the simulation tests converge to the consistent result, the computation were accepted.

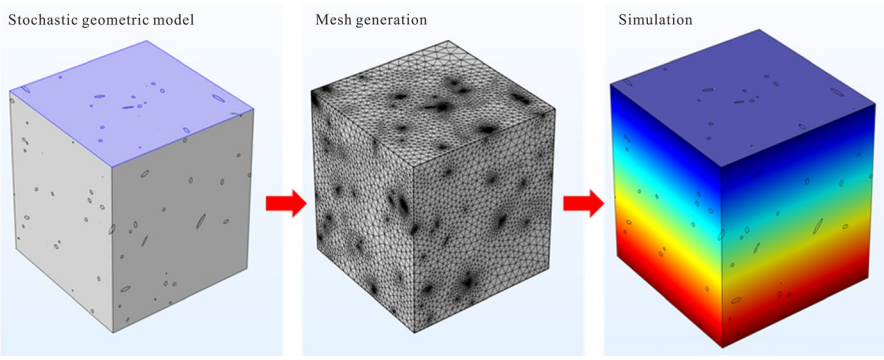

Fig. 2 The process of simulating the effect of porosity on thermal conductivity

2.1.2 Simulation Results

For each length of the semi-major axis, the software generates 20 different random geometries, calculates the effective thermal conductivity for each one separately, calculates its mean and standard deviation, and performs 20 operations for each semi-axis length to reduce the randomness of the simulation. The simulation results presented in Fig. 3 show that the effective thermal conductivity is constant at 2.74 $W{\cdot}m^{-1}{\cdot}K^{-1}$. However, the thermal conductivity fluctuates with the length of the semi-major axis, and the standard deviation tends to increase with the size of the ellipsoid. The relationship between pore size and rock thermal conductivity obtained from the simulations reported in this paper is analogous to the relationship between mineral particle size and thermal conductivity [10, 15]. Smaller particles have a larger internal contact area, leading to greater contact thermal resistance.

Suppose the total volume of the ellipsoid is 0.10 cm^3 so that semi-major axis of the ellipsoid is 0.009 cm, 0.009 cm … 0.20 cm, respectively, for finding the volume of the ellipsoid with different half-axis lengths and finding the total surface area of the ellipsoid at different half-axis lengths when the total volume reaches 0.10 cm^3 (Fig. 4). The number of ellipsoids and the total area (the surface areas of all the ellipsoids combined) decrease as the length of the semi-major axis increases. This supports a previous suggestion that the contact thermal resistance decreases with the addition of particles. In the range of semi-major axis lengths 0.009–0.0181 cm, the number of ellipsoids decreased by more than 20 000 for each 0.001 cm increase in length; in the range 0.0181–0.0199 cm, the number of ellipsoids decreased by more than 10 000 for each 0.001 cm increase in length; and in the range above 0.0199 cm,

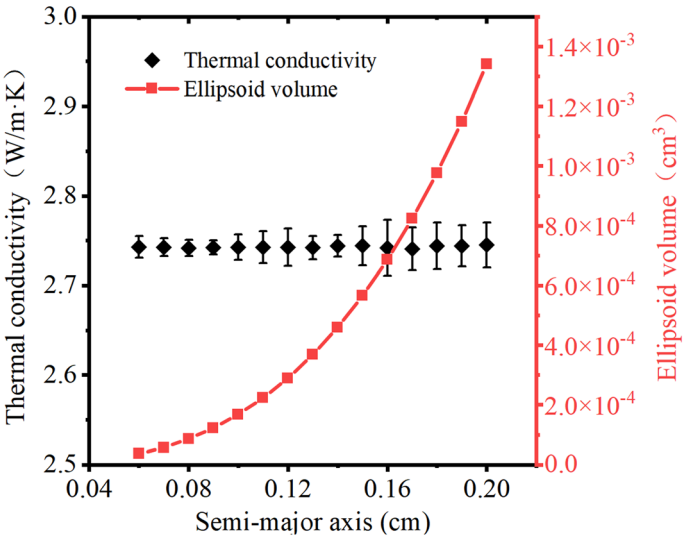

Fig. 3 The relationship among the semi-major axis, thermal conductivity and the volume of the individual ellipsoid. The error generally increases along the semi-major axis indicates that with the increase of particle size and the decrease of particle number, each particle has a greater impact on the whole temperature field, which can cause more uncertainties

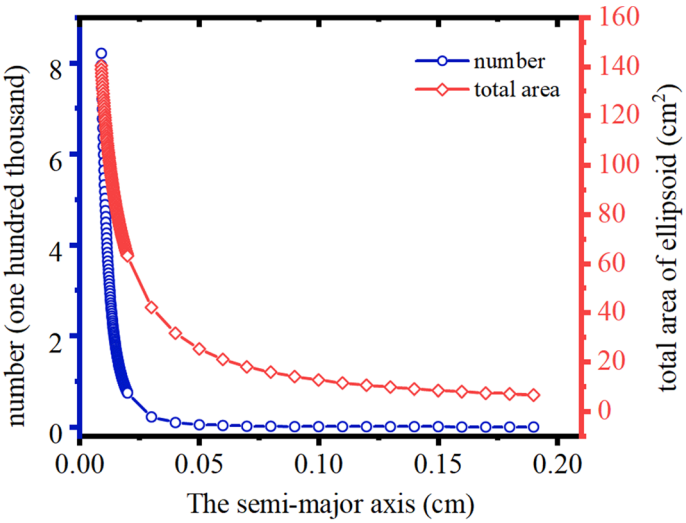

Fig. 4 Relationship among the semi-major axis, the number of ellipsoids and the total surface area of the ellipsoids

the number of ellipsoids decreased by an average of 4 117 for each 0.001 cm increase in length. The total area curve exhibits a similar trend to the number curve, although it is slightly flatter. Below 0.05 cm, the total area decreased rapidly as the semi-major axis increases, with an average rate of change of 2300 $cm^2 \cdot cm^{-1}$, while in the range greater than 0.05 cm, the total area decreased much more slowly, with an average rate of change of 135 $cm^2 \cdot cm^{-1}$. These trends show that there may be large differences in the contact thermal resistance between particles in rocks with different pore or particle sizes.

2.2 Effect of Fracture Angle on Thermal Conductivity

2.2.1 Modeling

We again used a square of 1 cm × 1 cm × 1 cm as the rock skeleton and calculated the thermal conductivity, density, and specific heat capacity of the material in the same way as above. We generated a parallel hexahedron 1 cm in length, 0.1 cm in width, and 1 cm in height in the center of the square as the fracture and filled it with air. At this point, the parallel hexahedron is oriented parallel to the direction of heat flow; i.e., at an angle of 0°. Then, in successive steps of 0.005 cm, we translated the upper surface one step to the left and the lower surface one step to the right, until the crack is finally translated to be perpendicular to the heat flow direction; i.e., at an angle of 90° (Fig. 5). We modeled the entire process 200 times and calculated the physical properties 200 times, generating 200 sets of data. The upper surface temperature of each model was 293.15 K, and the lower surface temperature was 273.15 K, so the temperature gradient was 20 $K \cdot cm^{-1}$.

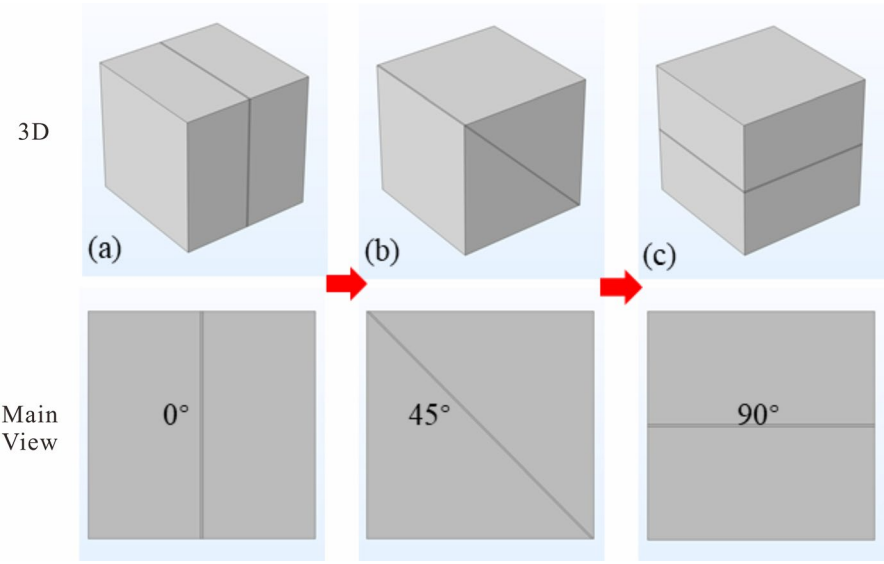

Fig. 5 Illustration of the process of modeling fracture angles

2.2.2 Simulation Results

Figure 6 shows the simulation results. As the fracture angle is increased, the thermal conductivity decreases monotonically. At the crack angle of 45°, the thermal conductivity decreased abruptly from 1.59 $W{\cdot}m^{-1}{\cdot}K^{-1}$ to 1.40 $W{\cdot}m^{-1}{\cdot}K^{-1}$. The change in the thermal conductivity with crack angle can be divided into two stages. In the first stage, from 0° to 45°, the thermal conductivity decreases faster and faster as the

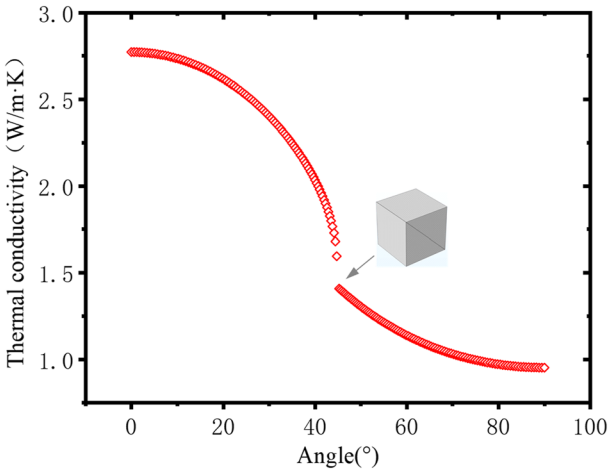

Fig. 6 Correlation of the thermal conductivity with the angle of the crack

angle increases, and the curve of thermal conductivity versus fracture angle is concave downward; the thermal conductivity decreases by 42.6 % in this stage. In the second stage, from 45 to 90°, the thermal conductivity continues to decrease as the angle increases, and the curve is convex upward. The thermal conductivity decreases by 40.3 % in this stage. This result indicates that in modeling the effective thermal conductivities of rocks, attention must be paid to the angular relationship between cracks and heat flow. There are differences in the thermal conductivity for cracks of the same nature but oriented at different angles from the direction of heat flow.

2.3 Influence of Component Arrangement on Temperature Effects

2.3.1 Modeling

Rocks are complex assemblages of components, and the main components of their skeletons include various minerals, rock debris, glassy substances, etc. The pore fluids include air, water, oil, gas, etc. The thermal conductivities of the different components may be quite different, and the thermal conductivity of each component also varies with external factors such as temperature and pressure. The combined arrangement of all these components makes the heat-conduction through rocks complicated. From the physical point of view, the components of a rock can be reduced to several thermal conductivity units whose volume fractions sum to one [16]. For example, a rectangular body can be constructed from five small rectangular pieces 1 cm in length, 1 cm in width, and 0.25 cm in height, as shown in Fig. 7.

This design approach ensures that the shape, size, and composition of the total block do not change when the five small blocks are arranged arbitrarily. To reflect the influence of the thermal conductivity of different compositions at different temperatures on the thermal conductivity of the bulk rock, we assume that the thermal conductivities of these blocks at room temperature (T_1) are significantly different than they are at some higher temperature (T_2) (Table 1), and we simulated the heat transfer through the entire block at these two temperatures separately. We used five different blocks with 120 randomly selected arrangements, and we simulated the thermal conductivities k_1 at T_1 and k_2 at T_2 for 20 of them.

2.3.2 Simulation Results

Assuming two conditions under a given temperature gradient (40 $K{\cdot}km^{-1}$), we simulated the heat flow densities q_1 and q_2 for different combinations at overall temperatures close to T_1 and T_2. We then calculated the overall bulk thermal conductivities k_1 and k_2 for each assemblage of blocks and the change of the thermal conductivity ($\Delta k/k_1$) between the two temperatures (Table 2). Table 2 and Fig. 8 show the change in the thermal conductivity as a function of arrangement. We label each arrangement of the five blocks as follows. In Fig. 7, A1, A2, A3, A4, and A5 represent the five blocks located in the five positions 1, 2, 3, 4, and 5, respectively. When block A_i is instead located in the first position, the first digit of the number for that particular arrangement is i, and the rest of the block

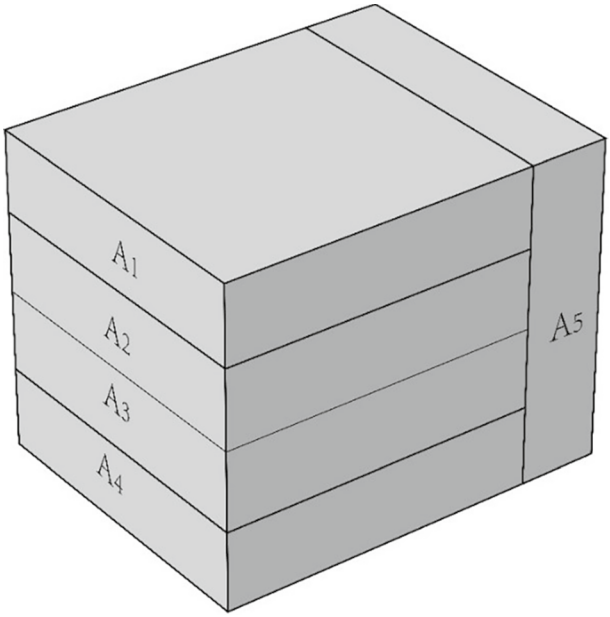

Fig. 7 Diagram of a bulk arrangement of five components

Table 1 Presupposed thermal properties of the designed components

Blocks	k_1(W·m^{-1}·K^{-1})	k_2(W·m^{-1}·K^{-1})	Change rate of k (%)	Density (kg·m^{-3})	Constant pressure heat capacity (J·kg^{-1}·K^{-1})
A1	5.0	3.0	− 40	2800	850
A2	6.0	1.0	− 83	2800	850
A3	9.0	7.0	+ 22	2800	850
A4	2.0	8.0	+ 300	2800	850
A5	4.0	1.0	− 75	2800	850

k thermal conductivity; k_1 k at room temperature; k_2 k at high temperature

numbers follow similarly. Figure 8 shows that the response to temperature of the thermal conductivity of the rock is different for the 20 different arrangements. At high temperatures, the thermal conductivity of the rock is lower than it is at room temperature; the decrease in the thermal conductivity ranges from − 50.3 % to − 36.7 %. In addition, the change of the thermal conductivity of the 5 components were exaggerated to reveal this influence mechanism of thermal conductivity which exists in nature, but difficult to detect, when the thermal conductivity changes little with temperature.

Table 2 Effective thermal conductivity of the combined bulk under different arrangements

No	Arrangement mode	q_1 (mW·m^{-2})	q_2 (mW·m^{-2})	k_1/(W·m^{-1}·K^{-1})	k_2/(W·m^{-1}·K^{-1})	$\Delta k/k_1$
1	12345	166.99	90.42	4.17	2.26	−0.46
2	12354	192.32	118.00	4.81	2.95	−0.39
3	12453	189.00	110.75	4.73	2.77	−0.41
4	21354	192.00	119.00	4.80	2.98	−0.38
5	54321	168.00	84.49	4.20	2.11	−0.50
6	24351	166.83	84.49	4.17	2.11	−0.49
7	32541	170.01	84.49	4.25	2.11	−0.50
8	52143	189.91	114.71	4.75	2.87	−0.40
9	42351	168.64	83.73	4.22	2.09	−0.50
10	41352	172.68	91.03	4.32	2.28	−0.47
11	24315	165.49	90.95	4.14	2.27	−0.45
12	13425	165.49	90.95	4.14	2.27	−0.45
13	31542	151.01	90.12	3.78	2.25	−0.40
14	42513	189.74	112.14	4.74	2.80	−0.41
15	35412	171.98	89.77	4.30	2.24	−0.48
16	25314	192.19	121.61	4.80	3.04	−0.37
17	31254	192.51	122.18	4.81	3.05	−0.37
18	25413	188.97	11ed4.15	4.72	2.85	−0.40
19	43215	166.99	90.42	4.17	2.26	−0.46
20	32514	192.55	119.55	4.81	2.99	−0.38

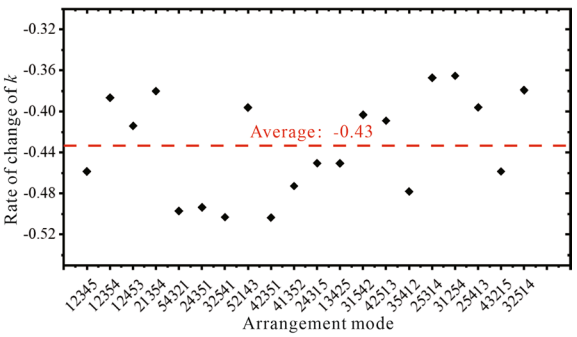

Fig. 8 Relationship between the change rate of the thermal conductivity and the arrangement modes

3 Discussion

In addition to previous knowledge about the influence of porosity and mineral composition on thermal conductivity, the results of this paper confirm that cracks, their angles relative to the direction of heat flow, and the arrangement of components with different responses to temperature have definite effects on the thermal conductivity of bulk rock. This understanding has reference value for modeling the thermal conductivity of fractured strata. In particular, it shows that thermal conductivity changes

before and after fracturing must be considered in the process of exploiting oil or gas reserves or in geothermal exploitation.

As porous media, heat transfer within subsurface rocks is diverse and includes seven different types of heat transport processes (see Fig. 9). Among them, thermal radiation becomes important only at temperatures above 900 °C. Since the temperatures of rocks located in sedimentary basins are generally no higher than 300 °C, thermal radiation does not need to be considered in studies at the basin scale. In addition, thermal convection needs to be considered only in studies of large-scale objects with apparent fluid activity—such as fracture zones or karst reservoirs—because thermal convection provides significant heat transfer only when there are large pores or strong fluid flow. In contrast, the pores of rocks are generally at the millimeter or micron scale, with low percolation rates. The effect of convective heat transfer can thus be ignored when studying the thermal conductivity of rocks.

Many models have been proposed to predict the thermal conductivity of rocks [8, 17–23]. They can be broadly classified into three categories: (1) theoretical models, (2) empirical models, and (3) hybrid theoretical–empirical models. Theoretical models strictly follow physical laws and employ mathematical derivations. However, they are very simplified and have limited scope for practical applications. An empirical model is obtained by fitting one or more empirical parameters that have some physical significance. Many scholars have proposed empirical models,

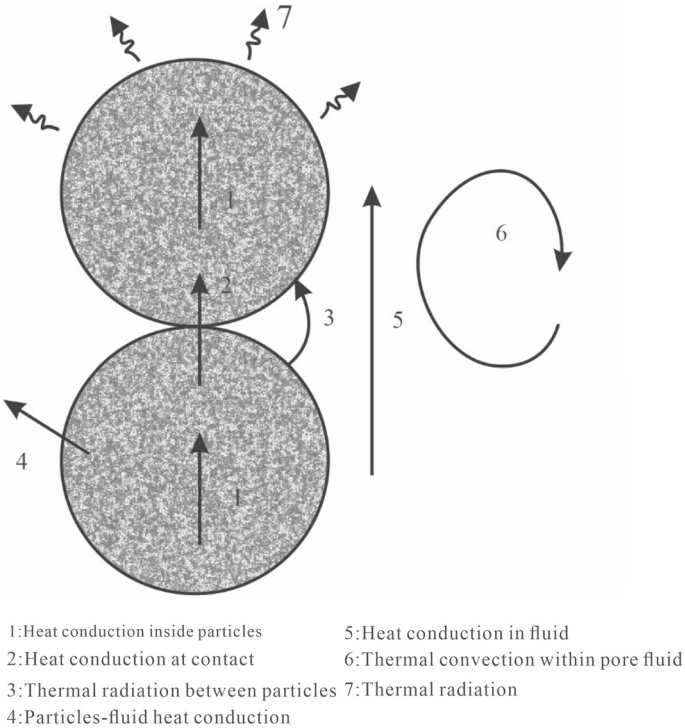

Fig. 9 Mechanisms of heat transport within rocks

which provide better fits for the samples used in modeling, but their portability is often poor. Hybrid theoretical–empirical models are ones in which the physical basis and empirical parameters are mixed; they combine both the physical basis of a theoretical model and the flexibility of an empirical model. Due to the complexity of rock compositions and the diversity of rock structures, the thermal conductivities of rocks are exceptionally complex [24], and they can fluctuate over a wide range, even for rocks of the same lithology [25, 26]. Studies of the thermal properties of rocks should therefore focus on systematic investigations of four aspects of the internal thermal conductivity mechanism of rocks: heat transfer within the rock skeleton, heat transfer between particles, heat transfer in fluids, and heat transfer between particles and fluids. The combination of theoretical simulations and experiments is clearly the general trend of future research, whether for rocks or other materials [27].

4 Conclusions

We found no obvious relationship between pore size and thermal conductivity at a given porosity, and the contact thermal resistance between rock particles with different pore or particle sizes may be significantly different. Conversely, the effect of the angle of a fracture relative to the direction of heat flow on the thermal conductivity is very significant. Specifically, the thermal conductivity decreases monotonically as the angle between the fracture and direction of heat flow increases, and the thermal conductivity is smallest when the fracture is perpendicular to the heat flow direction. The arrangement of the internal components of a rock also affects its thermal conductivity and its response to temperature, and it depends sensitively on the arrangement of the individual components.

Our results clearly demonstrate that attention needs to be paid to the angular relationship between fractures and heat flow and the *in situ* correction of thermal conductivity at high temperatures when modeling the effective thermal conductivity of shale or fractured formations. The thermal conductivity changes before and after fracture modification of a reservoir should be noted during the process of oil and gas or geothermal extraction. Accurate modeling of the rock thermal conductivity requires a combination of theoretical simulations and experimental analyses to investigate deeply the internal thermal conductivity mechanism of rocks.

Supplementary Information The online version contains supplementary material available at https://doi.org/10.1007/s10765-022-03132-8.

Acknowledgements We would like to show our appreciation to Dr. Xiaoning Shen and Ms. Zhengju Zhang from COMSOL Co. Ltd. for their guidance on the software operation.

Author Contributions CZ: the primary finisher of this paper; CC: coding and COMSOL simulation; XJ: completed part of the data processing work.

Funding The National Key Research and Development Program of China (Grant No. 2021YFA0716003) and the National Natural Science Foundation of China (Grant No. 42172334).

Data Availability The source codes are available for downloading at the following link: https://github.com/zhaoweiliu/-Stochastic-geometric-modelling/. Program language: JAVA. Software required COMSOL Multiphysics 5.0 and advanced versions. Program size: 7.13 KB.

Declarations

Conflict of interest The authors declare no conflict of interest.

References

1. Z.F. Duan, Z.H. Pang, F.T. Yang, Coal Sci. Technol. **41**, 15–17 (2013). https://doi.org/10.13199/j.cnki.cst.2013.08.008
2. Y.L. Zhang, T. Li, R.T. Mou, C.Z. Wang, F.C. Yuan, J. Qingdao Technol. Univ. **36**, 1–6 (2015)
3. L. Xiao, C.K. Yang, Z.H. Hu, X.Z. Li, M. Li, Rock Soil Mech. **31**, 86–91 (2010). https://doi.org/10.16285/j.rsm.2010.s2.006
4. S.S. Guo, C.Q. Zhu, N.S. Qiu, B.N. Tang, Y. Cui, J.T. Zhang, Y.H. Zhao, Energies **12**, 3884 (2019). https://doi.org/10.3390/en12203884
5. G.L. Wang, J. Gao, B.J. Zhang, Y.F. Xing, W. Zhang, F. Ma, Acta Geol. Sin. **94**, 1970–1980 (2020). https://doi.org/10.19762/j.cnki.dizhixuebao.2020235
6. X.G. Zhao, J. Wang, F. Chen, P.F. Li, L.K. Ma, J.L. Xie, Y.M. Liu, Tectonophysics **683**, 124–137 (2016). https://doi.org/10.1016/j.tecto.2016.06.021
7. Z. Abdulagatova, I.M. Abdulagatov, V.N. Emirov, Int. J. Rock Mech. Min. Sci. **46**, 1055–1071 (2009). https://doi.org/10.1016/j.ijrmms.2009.04.011
8. S.F. Wang, T. Wu, J. Eng. Thermophys. **37**(12), 2626–2630 (2016)
9. H. Liu, S. Ban, K. Bédard, B. Giroux, Adv. Geo Energy Res. **6**, 206–220 (2022). https://doi.org/10.46690/ager.2022.03.04
10. K. Midttomme, E. Roaldset, Petrol. Geosci. **4**, 165–172 (1998). https://doi.org/10.1144/petgeo.4.2.165
11. X.Q. Du, *Fundamentals of Numerical Simulation of Groundwater Flow* (China Water Power Press, Beijing, 2014)
12. C.J. Sun, Z.B. Han, Z. Zhen, Y. Fan, Environ. Eng. (2013). https://doi.org/10.7617/j.issn.1000-8942.2013.05.003
13. L. Gong, *2-D Finite Element Numerical Simulation of Geothermal Field* (Central South University, Changsha, 2014)
14. J.C. Wu, X.K. Zeng, X.B. Zhu, *Fundamentals of Numerical Simulation of Groundwater* (China Water Power Press, Beijing, 2017)
15. C. Chen, C.Q. Zhu, B.N. Tang, T.G. Chen, Prog. Geophys. **35**, 2047–2057 (2020). https://doi.org/10.6038/pg2020EE0013
16. R.W. Zimmerman, J. Petrol. Sci. Eng. **3**, 219–227 (1989). https://doi.org/10.1016/0920-4105(89)90019-3
17. Y. Popov, V. Tertychnyi, R. Romushkevich, D. Korobkov, J. Pohl, Pure Appl. Geophys. **160**, 1137–1161 (2003). https://doi.org/10.1007/PL00012565
18. U. Seipold, Phys. Earth Planet. Inter. **69**, 299–303 (1992). https://doi.org/10.1016/0031-9201(92)90149-P
19. I.H. Tavman, Int. Commun. Heat Mass Transf. **23**, 169–176 (1996). https://doi.org/10.1016/0735-1933(96)00003-6
20. M. Luo, J.R. Wood, L.M. Cathles, J. Appl. Geophys. **32**, 321–334 (1994). https://doi.org/10.1016/0926-9851(94)90031-0
21. C.M. Griffiths, N.R. Brereton, R. Beausillon, D. Castillo, Publications **65**, 299–315 (1992). https://doi.org/10.1144/GSL.SP.1992.065.01.23
22. F.W. Jones, F. Pascal, Geophysics **60**, 1038–1050 (1995). https://doi.org/10.1190/1.1443832
23. F. Pascal, F.W. Jones, Geophys. J. Int. **118**, 623–635 (1994). https://doi.org/10.1111/j.1365-246X.1994.tb03989.x
24. A.E. Ramazanova, Bull. Russ. Acad. Sci. Phys. **76**, 125–127 (2012). https://doi.org/10.3103/S1062873812010248

25. W.J. Cho, S. Kwon, J.W. Eng, Geology **107**, 167–171 (2009). https://doi.org/10.1016/j.enggeo.2009.05.012
26. I.M. Abdulagatov, Z.Z. Abdulagatova, S.N. Kallaev, A.G. Bakmaev, P.G. Ranjith, Int. J. Thermophys. **36**, 658–691 (2015). https://doi.org/10.1007/s10765-014-1829-4
27. M. Koru, K. Büyükkaya, Int. J. Thermophys. **43**, 155 (2022). https://doi.org/10.1007/s10765-022-03079-w

Authors and Affiliations

Chuanqing Zhu[1,2] · Chi Chen[1,2,3] · Xiaoxue Jiang[1,2]

Chi Chen
chenchigeosciences@foxmail.com

Xiaoxue Jiang
jiangxiaoxue135@163.com

[1] College of Geosciences, China University of Petroleum-Beijing, Beijing 102249, China

[2] State Key Laboratory of Petroleum Resources and Prospecting, China University of Petroleum-Beijing, Beijing 102249, China

[3] Guangzhou Marine Geological Survey, China Geological Survey, Guangzhou 510075, Guangdong, China